13A.4

# AN EXTENDED DUAL-DOPPLER RADAR STUDY OF THE HOUSTON RAINFALL AND LIGHTNING ANOMALIES

Lawrence D. Carey[1*], Veronica A. McNear[1], Michael L. Gauthier[2,3], and Walter A. Petersen[2]

[1] *Department of Atmospheric Sciences, Texas A&M University, College Station, Texas*

[2] *University of Alabama Huntsville, Huntsville, Alabama*

[3] *45th Weather Squadron, Patrick AFB, Florida*

## 1. INTRODUCTION

Cloud-to-ground (CG) lightning (Orville et al. 2001) and rainfall (Shepherd and Burian 2003) anomalies over and downwind of the Houston urban area have been well documented, especially over the summer season. Steiger et al. (2001) reported that CG lightning flash density over and downwind of the Houston area is enhanced by 45% above the background rural areas. Both Orville et al. (2001) and Steiger et al. (2001) hypothesize that anthropogenic effects such as aerosols or urban heat island (UHI) likely cause the lightning anomaly. Gauthier et al. (2005) confirmed that the CG flash density anomaly over Houston is a persistent and statistically significant although non-unique feature along the Gulf Coast during the summer. The non-unique nature of the lightning anomaly along the Gulf Coast suggests that mesoscale coastal impacts (e.g., sea breeze) could play an important role. Shepherd and Burian (2003) found that the largest rainfall amounts occur during the summer months, downwind of Houston. Shepherd and Burian (2003) suggest that the UHI's influence is of primary significance in causing the observed precipitation anomaly over and downwind of Houston. Burian and Shepherd (2005) determined that the highest ratio of rainfall between the Houston urban and the local rural areas occurs during the hours between 1200 and 1600 local time. The urban area experiences 59% more rainfall than the surrounding rural areas from noon to midnight and the downwind areas has a 30% greater rainfall amount for the same time period during the warm season.

In summary, there are well documented CG lightning and rainfall anomalies over and downwind of the Houston urban area that may be caused by one or more of the following hypothesized effects: 1) enhanced convergence, thermodynamic instability, or dynamical influences associated with the UHI; 2) altered microphysical processes associated with anthropogenic pollution; and/or (3) mesoscale enhancements in sea breeze convergence.

The placement of a Shared Mobile Atmospheric Research and Teaching Radar (SMART-R) near the KHGX Weather Surveillance Radar – 1988 Doppler (WSR-88D) during the 2005 summer season presents a unique opportunity to investigate the role of boundary-layer convergence in modulating convective frequency and intensity and thereby likely causing the rainfall and CG lightning anomalies. The relative roles of the urban heat island (UHI) and the sea-breeze as sources of low-level convergence leading to enhanced convection over Houston were also examined. Hourly average dual-Doppler winds and convergence were synthesized on 1 km2 horizontal grids for a nearly continuous eleven-week period. By using these analyses along with average CG lightning, rainfall, and reflectivity for a large Houston centered domain, it was possible to discern a correlation between low-level convergence and convection.

## 2. DATA AND METHODOLOGY

The Second Texas Air Quality Study (TexAQS II) was a comprehensive research initiative to better understand the causes of air pollution and, ultimately, to improve regulatory analysis of and prediction tools for ozone. Air pollution events are the consequence of both atmospheric chemistry and meteorological processes on local to regional scales. An important component of this research initiative was to provide enhanced meteorological measurements during an extended period over eastern Texas, including the urban environments of Houston-Galveston. A key objective of the enhanced meteorological monitoring was to quantify the transport into, within (including on urban scales), and out of Texas so that the formation and accumulation of ozone can be better predicted.

During the summer of 2005, a SMART radar was deployed to specifically sample boundary layer winds over the greater Houston-Galveston metropolitan areas. The SMART radars (Table 1 and Biggerstaff et al. 2005) are a collaborative effort between the National Severe Storms Laboratory, Texas A&M University, Texas Tech University, and the University of Oklahoma. The two SMART radars (SR-1 and SR-2) are C-band 5-cm mobile Doppler radars mounted on flatbed trucks.

SR-1 was deployed to the La Porte Municipal Airport almost 22 km due north of the KHGX WSR-88D location in League City, Texas. The 22-km dual-Doppler baseline provided excellent convective scale coverage of boundary layer winds over much of the Houston urban area, some of the surrounding rural area, and Galveston Bay (Fig. 1). SR-1 provided nearly uninterrupted Doppler radar coverage at this location

* *Corresponding author address*: Dr. Larry Carey, Dept. Atmospheric Sciences, Texas A&M University, College Station Texas 77843-3150; larry_carey@tamu.edu

from 9 July to 21 September 2005. This Doppler radar data set provides a unique opportunity to investigate the role of boundary-layer convergence in modulating convective frequency and intensity and thereby likely causing the rainfall and CG lightning anomalies.

**Table 1.** Basic SR-1 specifications and scan strategy.

| **Item** | **Description** |
|---|---|
| Wavelength | 5.5 cm |
| Polarization | Linear Horizontal (H) Polarization |
| Recorded data fields | Horizontal reflectivity ($Z_H$) and Radial Velocity ($V_R$) [Doppler Spectral Width($\sigma_D$) if desired] |
| Pulse Repetition Frequency (PRF) Unambiguous Velocity (Range) | 1200 Hz<br>16.5 m $s^{-1}$ (125 km) |
| Scan Type | 330° Plan Position Indicator (PPI) radar sector volumes (i.e., varying azimuthal sweeps at multiple fixed elevation angles) |
| Number of Samples | 64 pulses |
| Scan speed | 15 deg $s^{-1}$ |
| Fixed Elevation Angles ($\alpha$) | 0.5, 1.5, 2.5, 3.5, 4.5, 6.0° |
| Scan Time | ≈ 160 s (2.7 min) |

The SR-1 truck cab creates an approximate 30° azimuthal block of the antenna scan pattern. To mitigate the impact of the azimuthal cab block on boundary layer coverage, the SR-1 truck was pointed directly toward the KHGX radar (i.e., into the baseline) where horizontal winds cannot otherwise be retrieved. SR-1 was scanned in PPI volume mode through a 330° sector that was optimized for rapid boundary layer coverage (Table 1). When combined with the typical VCP-11, 21, or 31 KHGX volume coverage pattern (VCP), temporally coincident WSR-88D and KHGX volume start times were always less than 3-minutes apart, allowing for a reasonable dual-Doppler wind retrieval based on the quasi-steady approximation.

The data obtained from the SMART-R and WSR-88D data had to be translated from the radar coordinates (i.e., azimuth angle, elevation angle, range) in raw form, which are IRIS and Level II, respectively. This was done using the xltrsii data translator developed by the National Center for Atmospheric Research (NCAR).

The SR-1 and KHGX Doppler velocity data then had to be cleaned and unfolded, if necessary, using a combination of custom and NCAR software. An SR-1 radar gate with a spectrum width less than 0.7 m $s^{-1}$ or a velocity between -0.25 and 0.25 m $s^{-1}$ was considered to be ground clutter and was removed (i.e., a notch filter about zero mean motion was applied to the SR-1 velocity data). WSR-88D Doppler velocity data in Level II format has already been put through a clutter mitigation filter. In order for dual-Doppler processing to be done, the data were translated to Cartesian coordinates using the NCAR program REORDER (Oye and Case 1995). Grids of 1 km horizontal spacing, 200 m vertical spacing up to 2 km above ground level, 1 km horizontal radius of influence, and 400 m vertical radius of influence were made for convergence and wind maps. The vertical grid spacing and radius of influence were chosen to avoid sampling outside of the boundary layer while providing adequate horizontal coverage of the Houston area. Grids of 1 km horizontal and vertical resolution up to 10 km altitude with 1 km horizontal and vertical radii of influence were made for KHGX radar reflectivity analysis of precipitation features such as 2 km average reflectivity and convective frequency, 7 km average reflectivity and convective frequency, and rainfall. Rain rates (R) and hence domain averaged rainfall were estimated from gridded KHGX radar reflectivity using the tropical Z-R relationship ($Z=250R^{1.2}$) of Rosenfeld et al. (1993). The larger vertical radius of influence, grid spacing, and maximum grid level were chosen to increase vertical data coverage to retrieve convective reflectivity values aloft.

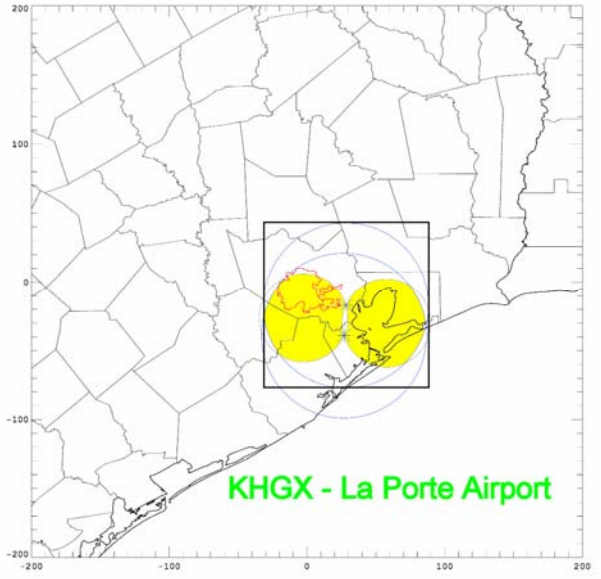


**Fig. 1.** Dual-Doppler analysis domain (yellow shading) formed by SR-1 (northern radar indicated by an asterisk) and KHGX (southern radar indicated by an asterisk). The Houston urban zone is indicated by the red outline. County and coastal boundaries areas are also shown. The dual-Doppler domain is formed by the intersection of the 20° beam crossing angle of the KHGX-SR-1 radar pair and the 60 km range rings from each radar. Synthesized horizontal winds in the boundary layer are available in the shaded yellow area. The overall analysis domain for radar reflectivity based parameters is indicated by the 120 km x 120 km box centered on SR-1. See Fig. 2 for more details.

The positioning of two radars in proximity to one another allows two-dimensional winds to be computed as described in Armijo (1969). The baseline between radars affects data resolution and range. Davies-Jones

(1979) shows that for a small baseline range and coverage areas are decreased, while data resolution is increased. As mentioned earlier, the distance between SR1 and KHGX is approximately 22 km. For typical boundary layer depths and minimum radar elevation angles in Table 1, the dual-Doppler lobes are confined to an area within approximately 60 kilometers of the radar to avoid sampling outside of the boundary layer. Furthermore, the sensitivity of SMART-R and WSR-88D to clear-air signatures is typically limited in range to about 60 km, regardless of boundary layer depth. Dual-Doppler synthesis was accomplished using the NCAR program Custom Editing and Display of Reduced Information in Cartesian space (CEDRIC) (Miller and Frederick 1998). When necessary, Doppler velocity unfolding was accomplished using a combination of local and global unfolding in REORDER and CEDRIC, respectively, according to the procedure of Miller et al. (1986). A 20° beam-crossing angle threshold was chosen to maximize the analysis domain of synthesized winds while maintaining acceptable error variances (Davies-Jones 1979). In clear-air conditions, it can be assumed that the vertical velocity near the surface is zero. The near surface zero vertical velocity can be used as a boundary condition for upward integration. Therefore, for the purpose of this study, upward integration was used with a boundary layer condition of a fraction of the calculated divergence. The particle terminal fall speed was assumed zero to reflect clear air conditions. On some occasions, the boundary layer contained convective echo. Even under precipitating conditions, the above assumptions are thought to result in negligible errors in the retrieved horizontal wind and calculated convergence due to the sin(α) dependence of the associated error. The retrieved boundary layer vertical motion was *not* used in this study.

The number of dual-Doppler radar volume times processed for this study was enormous (approximately every 10-minutes for nearly 11 weeks ≈ 11,000 volume times). To facilitate the Doppler processing of nearly 500 GBytes of SR-1 and KHGX radar data, a PERL script adapted from Dolan and Rutledge (2007) was used to automate all radar data processing in this study.

The National Lightning Detection Network (NLDN) is the source of cloud-to-ground (CG) lightning flash data for this study. The network consists of 106 sensors located around the United States which detect the time, location, peak current of the first return stroke, and flash multiplicity (or number of return strokes) per CG lightning flash (Cummins et al. 1998). The network detects peak currents of 4-5 kA or larger. A validation done in the upper Texas/Oklahoma region revealed median location accuracy of 282 m, and a stroke (flash) detection efficiency of 85% (92%) (Cummins et al. 2006).

Hourly domain averages of convergence (at 200 m AGL), 2-km reflectivity, 2-km convective frequency, 7-km reflectivity, 7-km convective frequency, rainfall, and CG lightning flash density were computed. Radar properties at 2 km are intended to gauge convection in general while those at 7 km are intended to provide a proxy for lightning potential (e.g., Vincent et al. 2004). Time series of these hourly quantities for the overall domain and several sub-domains (Fig. 2) will be presented and discussed in relation to the diurnal cycle.

The sub-domains were chosen to investigate the difference between the Houston and surrounding rural areas and also to help separate the UHI and sea-breeze sources of convergence. More specifically, the location of boxes 1 and 2 were chosen to analyze the influence of Houston on convergence and convection. Box 3 was selected because that contained comparable convective activity to boxes 1 and 2 but should not be influenced by the UHI effects of Houston. Box 4 was chosen to represent convection over the Galveston Bay and provide contrast to the three other sub-domains over land. Each box was made to be 900 km2. To compute the statistical significance of each sub-domain box compared to the domain mean a Wilcoxon rank-sum test at the 95% level of significance was used. This was preferable to the Student's t-test due to the non-normal distribution of the data. Results of not significant, significantly greater, or significantly less were gathered and presented in table form between the averages in each sub-domain box and the overall domain. Although most of the images are not shown here, overall and hourly average maps were also computed for all of these quantities during the course of the study.

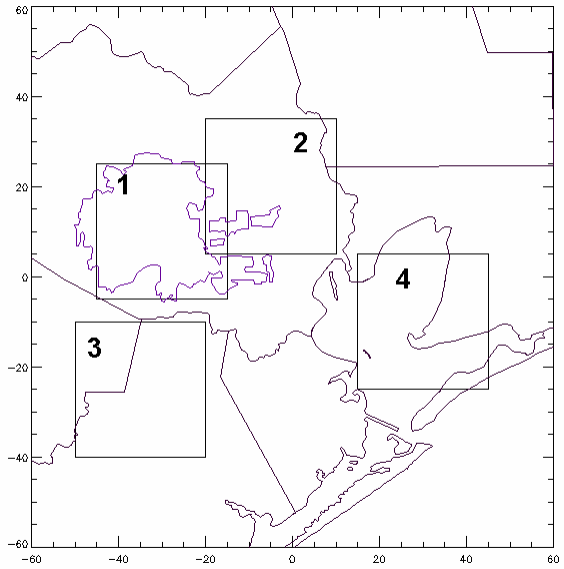


**Fig. 2.** Graphical representation of the overall analysis domain, which is the same as the boxed area in Fig. 1, and sub-domain boxes. Distance is in km relative to the location of SR-1. Houston urban, county, and coastal boundaries are shown.

Even after careful automated data processing, occasional ground clutter and other artifacts such as bird migrations persisted in the Doppler velocity data. The bird (purple martin) migrations were primarily limited to sunrise and sunset over a large park in southwest Houston. For example, a strong divergence signature was present in the retrieved velocities over the

park at sunrise when the roosting birds took flight to feed. The bird migration signatures in the synthesized Doppler velocities were manually removed during the worst periods. Furthermore, ground clutter, other artifacts, and synthesis errors along the periphery of the analysis domain in the retrieved winds were mitigated by using a standard outlier rejection filter before computing domain and sub-domain averages.

To compliment the less than one summer season of radar data in our study and provide some context regarding the generality of our 2005 results, we make use of the 7-year (1997-2003) KHGX June-July-August (JJA) radar reflectivity data base of Gauthier et al. (2006) to analyze the 30-dBZ convective frequency over the Houston area.

## 3. RESULTS

Figure 3 presents a time series plot of boundary layer convergence for each box and the domain. Both the domain and box 1 are presented with and without the filter for birds. The overall domain pattern was convergence from 20 LST (local standard time) overnight to 11 LST, followed by divergence. Box 1 shows continual convergence at all hours, except at times when birds are known to exist, 6 and 21 LST. Box 1, with the bird signal removed, greatly decreases the divergence associated with the bird signal, though it does not remove it completely. The convergence rose from midnight and peaked at 9 LST at 0.25 X $10^{-4}$ $s^{-1}$. Convergence then fell and stayed steady until 17 LST, at which point convergence slowly began to increase. Box 1 convergence was greater than the domain average at all times, with the greatest difference occurring at 8 and 9 LST. The average for Box 4 was convergent from 20 LST through the overnight hours until approximately 9 LST, at which time divergence began.

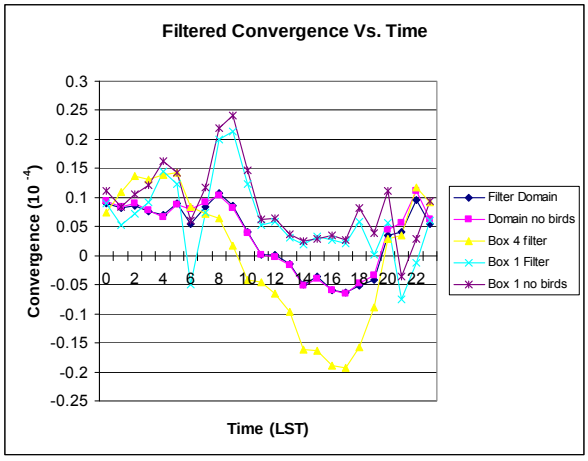


**Fig. 3.** Time series of boundary layer convergence at 200 m AGL ($10^{-4}$ $s^{-1}$) for the domain, bird edited domain, box 1, bird edited box 1, and box 4.

Table 2 presents the Wilcoxon Rank-Sum test between each box and the domain. Average convergence over box 1 (Houston) shows the trend of being significantly greater than the overall domain from the hours of 8 to 20 LST, significantly lower at 21 and 22 LST, and not significantly different from 23 overnight to 3 LST. Box 4 (Galveston Bay) shows the trend of being significantly lower than the domain average from 8 to 19 LST, not significantly different at 20 and 21 LST, and significantly greater from 1 to 5 LST.

**Table 2.** Hourly Wilcoxon Rank-Sum at 5% significance level results for box 1 and box 4 average convergence. N is not significantly different, H is significantly higher, and L is significantly lower as compared to the overall domain shown in Fig. 2.

| Hour (LST) | 0 | 1 | 2 | 3 | 4 | 5 | 6 | 7 | 8 | 9 | 10 | 11 |
|---|---|---|---|---|---|---|---|---|---|---|---|---|
| Box 1 | N | N | N | N | H | N | L | N | H | H | H | H |
| Box 4 | N | H | H | H | H | H | N | N | L | L | L | L |

| 12 | 13 | 14 | 15 | 16 | 17 | 18 | 19 | 20 | 21 | 22 | 23 |
|---|---|---|---|---|---|---|---|---|---|---|---|
| H | H | H | H | H | H | H | H | H | L | L | N |
| L | L | L | L | L | L | L | L | N | N | H | H |

Time series plots for average radar reflectivity at 2 km altitude over the four boxed areas and the entire domain are presented in Fig. 4. The domain mean shows a decrease in convection intensity overnight to early morning, with the overall minimum in intensity occurring at 4 LST of 14 dBZ. Convective strength increased and then reached a peak of 36 dBZ at 14 LST. A second minimum of near 15 dBZ was evident at 22 LST. Convection in box 1 showed a similar pattern, but convection was stronger during the overnight hours (23-3 LST), weaker from 4-9 LST, and similar to slightly stronger than the domain mean from 12-19 LST. The box 2 pattern was very similar to box 1 with the exception that the box 2 mean decreased earlier in the day, at 17 LST, and reached a lower minimum of 10 dBZ slightly earlier at 20 LST. Box 3 was also similar to box 1 except that the diurnal maximum appeared to be delayed to the early evening (18 LST). Convective intensity was slightly higher than box 1 for the hours of 17 and 18 LST, and lower at 23 LST. The pattern in box 4 was more unique. Convection was weaker in the mean than the domain until 4 LST. Convective in box 4 rose to 30 dBZ at 5 LST and remained fairly steady until 16 LST, although there was a slight tendency for stronger convection to occur in the morning hours between 06 and 12 LST. Convective strength began to slowly decrease and remained lower than all other boxes, with one exception at 20 LST, until 21 LST.

Table 3 presents the Wilcoxon rank-sum test for each box. The mean 2 km reflectivity for box 1 was significantly higher than the domain mean between 14 and 19 LST, and 23 to 3 LST. It was significantly lower

for the times of 6 to 9 LST and 11 to 13 LST. The box 2 average was significantly lower than the domain average from 17 to 21 LST. Box 3 was also very similar to box 1. However, box 3 was significantly lower than the domain average from 13 to 15 LST. Box 4 was only significantly higher than the mean from 4 to 9 LST, it was significantly lower at all other times.

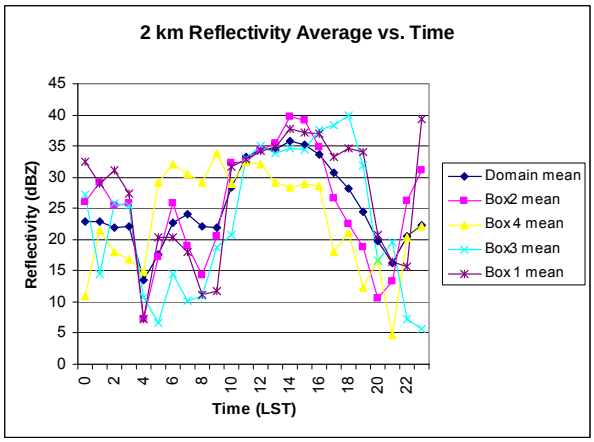


**Fig. 4.** Time series plot of domain and box average reflectivity (dBZ) at 2 km altitude.

**Table 3.** Hourly Wilcoxon Rank-Sum at 5% significance results for box average radar reflectivity, which was used as a proxy for convective intensity, at 2 km. N indicates not significantly different, H is significantly higher, and L is significantly lower than the domain mean.

| Hour (LST) | 0 | 1 | 2 | 3 | 4 | 5 | 6 | 7 | 8 | 9 | 10 | 11 |
|---|---|---|---|---|---|---|---|---|---|---|---|---|
| Box 1 | H | H | H | H | L | H | L | L | L | L | H | L |
| Box 2 | N | H | H | H | L | N | H | L | L | L | H | L |
| Box 3 | H | L | N | H | L | L | L | L | L | L | L | H |
| Box 4 | L | L | L | L | H | H | H | H | H | H | L | L |

| 12 | 13 | 14 | 15 | 16 | 17 | 18 | 19 | 20 | 21 | 22 | 23 |
|---|---|---|---|---|---|---|---|---|---|---|---|
| L | L | H | H | H | H | H | H | N | N | L | H |
| L | H | H | H | N | L | L | L | L | L | H | H |
| H | L | L | L | H | H | H | H | L | H | L | L |
| L | L | L | L | L | L | L | L | L | L | L | N |

Figure 5 presents time series of the domain and box averages for the frequency of convection at 2 km. Domain frequency was about 5 or 6 percent (about 2 to 3 events) from midnight until a minimum of near 2 percent (1 event) at 4 LST. From this time, domain average convective frequency increased to a maximum of near 18 percent at 14 LST. The convective frequency then began to drop and reached a steady level of near 4 percent at 20 LST until midnight. The overall pattern in box 1 was similar to the domain average. The frequency after midnight was slightly higher than the domain average, about 7-11 percent. The convective frequency then dropped to about 2 percent until 10 LST, at which point it began to rise. Box 1 convective frequency reached a maximum of 33 percent at 14 LST, which is the largest value of any of the regions. After this time, convective frequency in box 1 began to decrease. Convective frequency in box 2 was nearly identical to box 1. The maximum in box 2 was not as high as box 1, only 27 percent, and the frequency in box 2 decreased more rapidly than box 1, and reached a fairly steady minimum of 3 to 5 percent at 18 LST. Convective frequency in box 3 was also very similar to box 1. The maximum occurred slightly later, at 16 LST, and was lower, 21 percent. The convective frequency in box 4 was much lower than the frequency in all other boxes and exhibited a markedly different diurnal cycle. Box 4 frequency was very low, about 2 to 4 percent from midnight until 5 LST. At 5, the frequency was higher than any other box. The maximum for box 4 was at 7 LST at 11 percent. The frequency over box 4 slowly declined over the course of the day and reached a steady minimum of 2 percent at 18 LST until 22 LST.

Table 4 presents the results of the Wilcoxon rank-sum test for the domain and all boxes. The mean 2 km convective frequency for box 1 was significantly higher than the domain mean for almost all hours except 5 to 12 LST. Box 2 significance was generally similar to box 1. However, the mean for box 2 was significantly lower than the domain mean from 16 to 20 LST. Box 3 was different from box 1 during the hours of 22 LST overnight to 2 LST, at which times it was either significantly lower, or not significantly different, from the domain mean. Box 4 was only significantly higher than the domain mean between the hours of 5 to 9 LST.

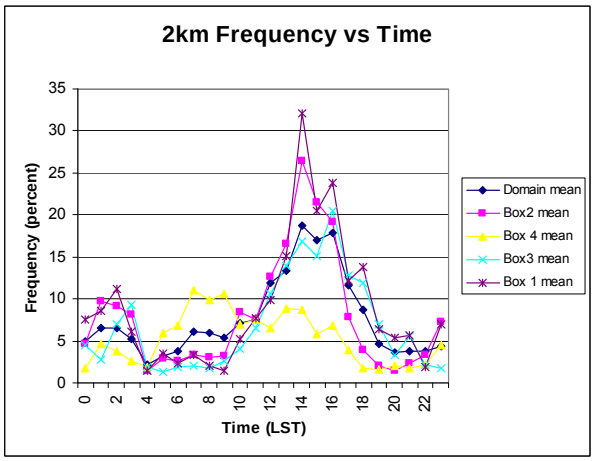


**Fig. 5.** Time series plot of domain and box convective frequency at 2 km altitude.

A time series plot for 7 km average reflectivity is presented in Fig. 6. The domain mean averaged around 10 dBZ near midnight. The domain average hit a minimum in average reflectivity at 4 LST, and began to rise to a maximum of 28 dBZ at 14 LST. Reflectivity values then decreased steadily until 21 LST. The box 1 pattern was very similar to the domain mean. Box 1 values were approximately 5 dBZ higher at midnight and then dropped off to 0 to 5 dBZ during the time span of 4 to 9 LST. The peak of about 32 dBZ in 7 km reflectivity occurred at 14 LST. Reflectivity values did not begin to drop until 19 LST, after which there was a small increase in reflectivity values. Box 2 was very similar to box 1 values, with the nearly the same overall pattern. Box 2 mean reflectivity aloft reached a maximum of 35 dBZ at 14 LST. However, box 2 mean reflectivity values at 7 km decreased rapidly after the peak. Box 3 was also very similar to box 1; however, the peak of 35 dBZ was reached later at 18 LST, after which there was a rapid decrease in reflectivity, reaching 0 dBZ at 22 LST. The box 4 mean reflectivity value aloft was similar to the other boxes near midnight, but average reflectivity rose much earlier in the day. A peak of near 27 dBZ was reached at 7 LST in the morning. Mean reflectivity values at 7 km remained fairly steady until 16 LST, at which point they decreased to 0 dBZ by 21 LST.

**Table 4.** Same as Table 3 except for box average convective frequency at 2 km altitude.

| Hour (LST) | 0 | 1 | 2 | 3 | 4 | 5 | 6 | 7 | 8 | 9 | 10 | 11 |
|---|---|---|---|---|---|---|---|---|---|---|---|---|
| Box 1 | H | H | H | H | L | H | L | L | L | L | L | N |
| Box 2 | H | H | H | H | L | N | L | L | L | L | H | H |
| Box 3 | N | L | N | H | N | L | L | L | L | L | L | L |
| Box 4 | L | L | L | L | L | H | H | H | H | H | N | L |

| 12 | 13 | 14 | 15 | 16 | 17 | 18 | 19 | 20 | 21 | 22 | 23 |
|---|---|---|---|---|---|---|---|---|---|---|---|
| L | H | H | H | H | H | H | H | H | H | H | H |
| H | H | H | H | L | L | L | L | L | H | H | H |
| H | H | L | L | H | H | H | H | N | H | L | L |
| L | L | L | L | L | L | L | L | L | L | L | N |

Table 5 presents the results of the Wilcoxon rank-sum test for 7 km mean reflectivity. The mean for box 1 was significantly higher than the domain mean between the hours of 12 and 19 LST, and was significantly lower between 6 and 9 LST. Box 2 was similar, but was only significantly higher between 12 and 16 LST, and was significantly lower between 19 to 21 LST and 7 to 9 LST. Box 3 was significantly higher from 11 to 14 LST and 16 to 20 LST, and was significantly lower from 4 to 10 LST. Box 4 was significantly higher from 5 to 11 LST and was significantly lower from 12 to 21 LST.

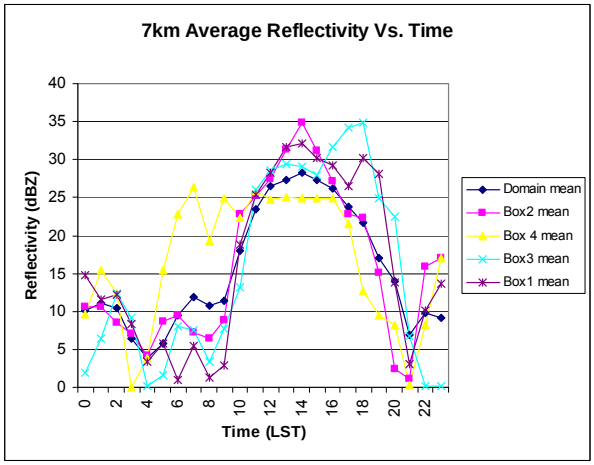


**Fig. 6.** Time series of domain and box averaged reflectivity (dBZ) at 7 km altitude.

**Table 5.** Same as Table 3 except for box average radar reflectivity at 7 km altitude.

| Hour (LST) | 0 | 1 | 2 | 3 | 4 | 5 | 6 | 7 | 8 | 9 | 10 | 11 |
|---|---|---|---|---|---|---|---|---|---|---|---|---|
| Box 1 | H | N | H | H | N | N | L | L | L | L | H | N |
| Box 2 | N | L | L | N | N | H | N | L | L | L | H | N |
| Box 3 | L | L | H | H | L | L | L | L | L | L | L | H |
| Box 4 | N | H | H | L | N | H | H | H | H | H | H | H |

| 12 | 13 | 14 | 15 | 16 | 17 | 18 | 19 | 20 | 21 | 22 | 23 |
|---|---|---|---|---|---|---|---|---|---|---|---|
| H | H | H | H | H | H | H | H | L | L | N | H |
| H | H | H | H | H | L | N | L | L | L | H | H |
| H | H | H | N | H | H | H | H | H | N | L | L |
| L | L | L | L | L | L | L | L | L | L | H | N |

A diurnal time-series of convective frequency for reflectivity values above 30 dBZ at 7 km altitude is presented in Fig. 7. The plot shows that the count was near zero for all boxes and the domain between midnight and 4 LST. The domain count remained near zero until 9 LST and then slowly increased to a peak of near 2.5 at 14 LST, and slowly began to decrease after that time. Box 1 also did not increase until after 9 LST, but increased rapidly and reached a peak of near 6.5 at 14 LST. Box 1 then decreased, but has another small peak at 19 LST, after which the frequency decreased to

near zero at 21 LST. Box 2 was almost identical to box 1, but did not achieve a second peak and dropped to near zero by 17 LST. Box 3 increased slowly after 9 LST and reached a peak of near 4 at 16 LST. Counts for box 3 stayed fairly steady until after 18 LST, when counts dropped to near zero. Box 4 counts began to rise after 4 LST, and remained fairly steady between 0.5 and 1 until 17 LST.

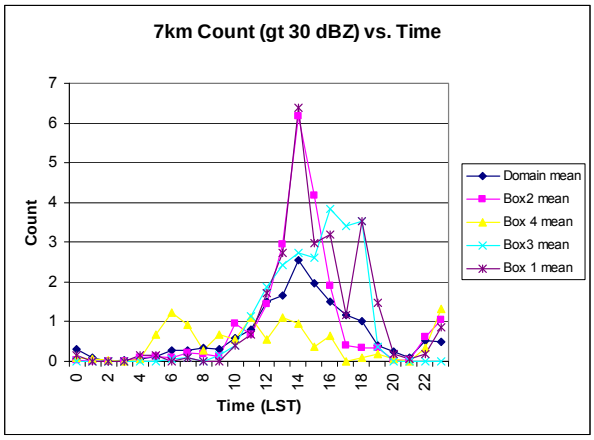


**Fig. 7.** Time-series of domain and box average convective frequency for reflectivities above 30 dBZ at 7km altitude.

**Table 6.** Same as Table 3 except for the box average convective frequency for reflectivities above 30 dBZ at 7 km altitude.

| Hour (LST) | 0 | 1 | 2 | 3 | 4 | 5 | 6 | 7 | 8 | 9 | 10 | 11 |
|---|---|---|---|---|---|---|---|---|---|---|---|---|
| Box 1 | N | L | N | N | H | N | L | L | L | L | N | N |
| Box 2 | L | L | N | N | N | N | L | L | L | L | H | N |
| Box 3 | L | L | N | N | L | L | L | L | L | L | L | H |
| Box 4 | L | N | N | N | N | H | H | H | N | H | N | H |

| 12 | 13 | 14 | 15 | 16 | 17 | 18 | 19 | 20 | 21 | 22 | 23 |
|---|---|---|---|---|---|---|---|---|---|---|---|
| H | H | H | H | H | H | H | H | L | N | L | H |
| N | H | H | H | H | L | L | N | L | L | H | H |
| H | H | H | N | H | H | H | H | L | L | L | L |
| L | L | L | L | L | L | L | L | L | L | N | H |

Table 6 presents the results of the Wilcoxon rank-sum test for convective frequency for reflectivities above 30 dBZ. The box 1 mean was significantly higher than the domain mean between 12 and 19 LST and was significantly lower between 6 and 9 LST. Box 2 was significantly higher between 13 and 16 LST, significantly lower between 6 and 9 LST, and was not significantly different from the domain mean between 2 and 5 LST. Box 3 was significantly higher between 11 and 14 LST and 16 and 19 LST, and was significantly lower between 20 overnight to 2 LST and 4 and 10 LST. Box 4 was significantly higher between 5 and 7 LST, was significantly lower between 12 and 21 LST, and was not significantly different between 1 and 4 LST.

Figure 8 presents a map of the total count of the occurrence of reflectivity above 30 dBZ at 7 km altitude. The highest counts occurred over downtown, northwest, and northeast of Houston. West of the radar cone of silence there was another large area of high frequency. Moderate and high counts were located in the northeast and northwest portions of the domain. The lowest frequencies occurred over the southern portion of Galveston Bay, over the Gulf of Mexico, and north of the east half of Galveston Bay. The results of the Wilcoxon rank-sum test show that the means of boxes 1, 2, and 3 were significantly higher than the domain mean while the mean of box 4 was significantly lower.

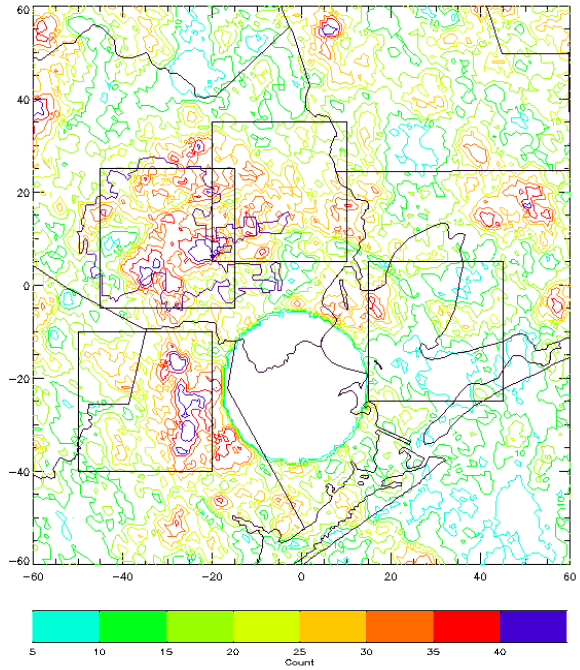


**Fig. 8.** Map of the frequency of convection for reflectivities above 30 dBZ at 7 km altitude.

Figure 9 presents a time series of average cumulative rainfall for each box and the domain. The domain average slowly rose after 4 LST, after a minimum of near 1 mm. The domain average reached a steady average of near 5 mm by 11 LST and did not drop until 20 LST. A peak of 7 mm was reached again at 23 LST. The box 1 pattern was similar, but was characterized by larger values at 16, 18, and 19 LST, at which time a peak of 20 mm average rainfall was reached. A second peak of 24 mm occured at 23 LST after dropping to near 0 between 20 and 22 LST. The

average in box 2 was higher at 14 and 15 LST than box 1. A first peak of 8 mm occurred at 15 LST, and a second peak of 16 mm occurred at 23 LST. The pattern in box 3 was also similar to box 1 and box 2. Box 3 reached a peak value of 17 mm at 18 LST. Box 4 values rose from near zero to about 5 mm at 5 LST. The average value remained near 3 mm and decreased to near zero by 21 LST.

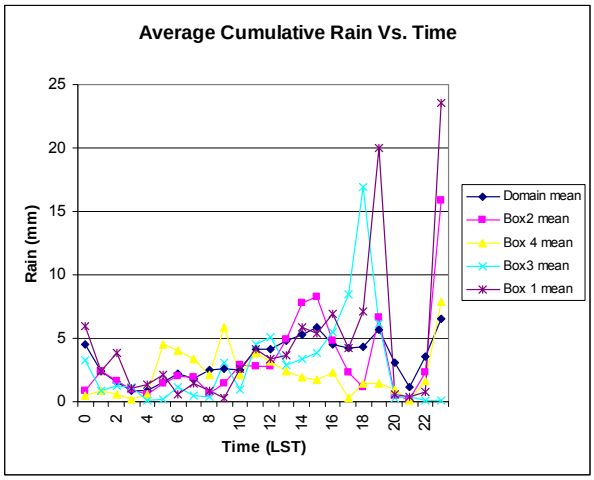


**Fig. 9.** Time series of domain and box average cumulative rainfall (mm).

**Table 7.** Same as Table 3 except for the box average cumulative rainfall.

| Hour (LST) | 0 | 1 | 2 | 3 | 4 | 5 | 6 | 7 | 8 | 9 | 10 | 11 |
|---|---|---|---|---|---|---|---|---|---|---|---|---|
| Box 1 | H | H | H | H | L | H | L | L | L | L | H | H |
| Box 2 | N | H | H | H | L | N | H | L | L | L | L | L |
| Box 3 | H | L | H | H | L | L | L | L | L | L | L | N |
| Box 4 | L | L | L | L | H | H | H | H | H | H | L | L |

| 12 | 13 | 14 | 15 | 16 | 17 | 18 | 19 | 20 | 21 | 22 | 23 |
|---|---|---|---|---|---|---|---|---|---|---|---|
| L | N | H | H | H | H | H | H | N | N | L | H |
| L | H | H | H | N | L | L | L | L | L | H | H |
| H | L | L | L | H | H | H | H | L | H | L | L |
| L | L | L | L | L | L | L | L | L | L | L | N |

Table 7 presents the results of the Wilcoxon rank-sum tests for average cumulative rainfall in each box. The box 1 mean was significantly higher than the domain mean from 14 to 19 LST and 23 LST to 3 LST and was significantly lower from 6 to 9 LST. Box 2 was significantly higher from 13 to 15 LST and 22 to 3 LST, and was significantly lower from 7 to 12 and 17 to 21 LST. Box 3 was significantly higher from 16 to 19 LST and significantly lower from 4 to 10 and 13 to 15 LST. Box 4 was significantly higher from 4 to 9 LST and significantly lower for all but one hour from 10 to 3 LST.

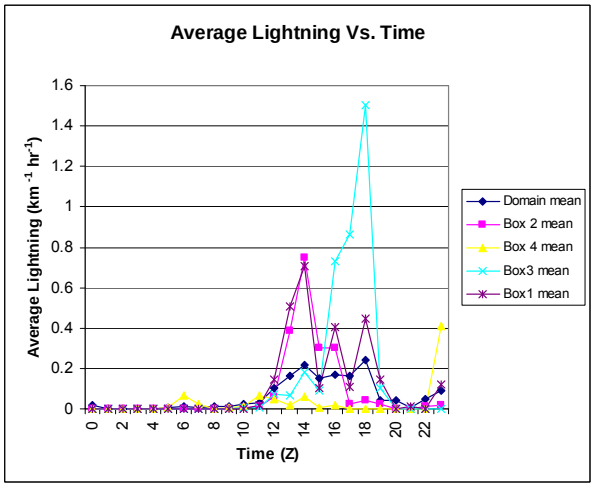


**Fig. 10.** Hourly time series of average CG lightning flash density ($km^{-1}$ $hr^{-1}$).

Figure 10 presents the hourly time series for mean CG lightning flash density. The domain mean was near zero $km^{-1}$ $hr^{-1}$ until 11 LST. The domain mean increased during the following two hours and reached a steady level of near 0.2 $km^{-1}$ $hr^{-1}$ until 19 LST at which point the mean decreased back to zero. Box 1 increase from 0 km-1 hr-1 at the same time of day as the domain, but increased sharply and reached a peak of 0.7 $km^{-1}$ $hr^{-1}$ at 14 LST. A second and third peak of near 0.4 $km^{-1}$ $hr^{-1}$ was reached at 16 and 18 LST, respectively. The box 1 mean returned to zero at 20 LST. Box 2 was nearly identical to box 1 and reached a similar peak as Box 1. Box 2 did not have any secondary peaks and decreased to zero by 17 LST. Box 3 slowly increased after 11 LST and sharply increased after 15 LST. Box 3 reached a peak of 1.5 $km^{-1}$ $hr^{-1}$ at 18 LST, and returned to zero at 19 LST. Box 4 remained near zero during each hour except 23 LST, at which point a peak of 0.4 $km^{-1}$ $hr^{-1}$ was reached.

Table 8 present the results of the Wilcoxon rank-sum test for average ground flash density. The box 1 mean was only significantly higher than the domain mean at 12 to 14, 16, 18, 19, and 23 LST. The mean was not significantly different from the domain mean at all other times. The box 2 mean was significantly higher between 13 and 16 LST, significantly lower at 17 and 18 LST, and not significantly different from the domain mean at all other times. The box 3 mean was significantly higher at 14 and 16 to 19 LST, significantly lower at 13 and 23 LST, and not significantly different from the domain mean at all other hours. The box 4 mean was only significantly higher at 23 LST, significantly lower from 12 to 18 LST, and not

significantly different from the domain mean at all other times.

**Table 8.** Same as Table 3 except for the box average CG lightning flash density.

| Hour (LST) | 0 | 1 | 2 | 3 | 4 | 5 | 6 | 7 | 8 | 9 | 10 | 11 |
|---|---|---|---|---|---|---|---|---|---|---|---|---|
| Box 1 | N | N | N | N | N | N | N | N | N | N | N | N |
| Box 2 | N | N | N | N | N | N | N | N | N | N | N | N |
| Box 3 | N | N | N | N | N | N | N | N | N | N | N | N |
| Box 4 | N | N | N | N | N | N | H | N | N | N | N | N |

| 12 | 13 | 14 | 15 | 16 | 17 | 18 | 19 | 20 | 21 | 22 | 23 |
|---|---|---|---|---|---|---|---|---|---|---|---|
| H | H | H | N | H | N | H | H | N | N | N | H |
| N | H | H | H | H | L | L | N | N | N | N | N |
| N | L | H | N | H | H | H | H | N | N | N | L |
| L | L | L | L | L | L | L | N | N | N | N | H |

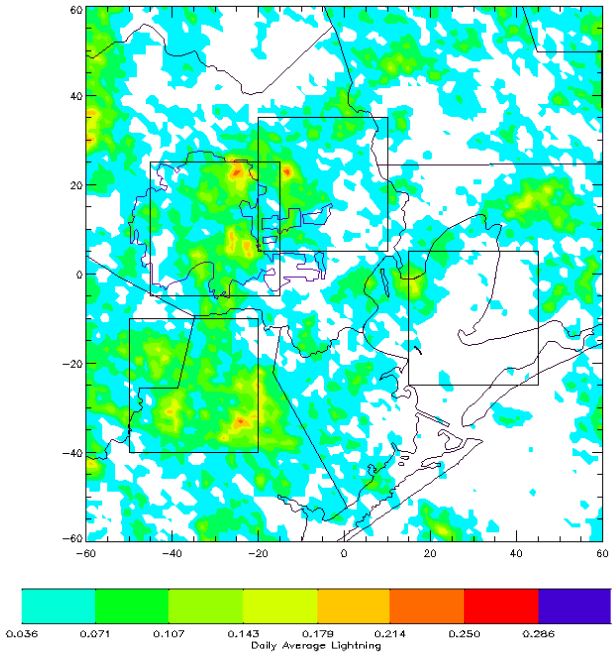


**Fig. 11.** Daily average CG lightning flash density (km$^{-1}$ day$^{-1}$).

Figure 11 presents the daily average lightning. Over downtown Houston maximum CG density reached 0.214 lightning flashes km$^{-1}$ day$^{-1}$. North and northeast of downtown, CG density reached 0.250 lightning flashes km$^{-1}$ day$^{-1}$. South of Houston also experienced high CG flash density also reaching 0.250 km$^{-1}$ day$^{-1}$. Most of the domain averaged 0.036 and 0.071 flashes km$^{-1}$ day$^{-1}$. Large areas of no CG lightning activity include directly north of the Houston area, off shore of Galveston Bay and the central and southern portions of Galveston Bay. Lightning activity was present along the northern coast of Galveston Bay. The results of the Wilcoxon rank-sum test show that the means for boxes 1, 2, and 3 were significantly higher than the domain mean while the mean for box 4 was significantly lower.

## 4. DISCUSSION

The following discussion will analyze the patterns that were present in the convergence field relative to convective properties. Identifiable patterns that could be associated with the sea-breeze and the urban heat island will be discussed. The correlations between the convergence patterns and the convective frequency and intensity will be examined, along with correlations between convective strength, rainfall, and the presence of lightning.

### *4.1 Convergence and UHI*

The location of boxes 1 and 2 were chosen to analyze the influence of Houston on convergence and convection. Box 3 was selected as an area that contained with comparable convective activity to boxes 1 and 2, but that should not be influenced by the UHI effects of Houston. The presence of convergence over most of the Houston area during the overnight hours as well as in the day indicates the presence of the UHI (Oke 1987). The UHI effect is more pronounced during the evening hours. South of Houston, there appears to be more divergence during almost all hours than over the Houston area. It is hard to be certain of the divergence due to the presence of radar artifacts in this area. During the overnight hours, there was a drop in convection in boxes 1, 2, and 3. The lack of convection during the overnight hours despite increased convergence in box 1, specifically, is likely due to the decrease of favorable thermodynamics during the overnight hours. Due to increased convective inhibition in the evening, there was most likely insufficient lifting for parcels to reach the LFC. However, this cannot be verified due to the lack of sounding data for Houston.

Reviewing the results in the prior section, we see that convergence values in box 1 peaked at 9 LST, and values peaked at 8 LST for boxes 2 and 3. Also, the peak values for 2 and 3 were nearly 0.15 X 10$^{-4}$ s-1 (60%) less than the peak for box 1. Convection in boxes 1, 2, and 3 increased dramatically between 9 and 10 LST. After this time, convergence decreases in all boxes until approximately 18 LST. This decrease in convergence is expected after the advent of convection due to rainfall, negative temperature perturbations (not shown), and downdraft divergence (e.g., seen in loops of velocity vectors for individual storms but not shown here). The strength of convection was approximately

the same for all times in late morning and afternoon for all three boxes and for both 2 km and 7 km. However, between the times of 17 and 19 LST, the strength of the convection in box 1 and box 3 remained high while the strength of the convection in box 2 began to decrease. The frequency of all events measured by the 2 km frequency was very similar across all 3 boxes. Box 2 decreased more quickly than box 1 and 3. Deep convection, measured by the count of above 30 dBZ at 7 km was over 2 times more frequent for boxes 1 and 2 than for box 3 at the peak at 14 LST. The drop in the frequency and strength of convection in box 2 after this time, while box 1 and box 3 maintain higher frequency and strength is most likely due to the proximity of box 2 to the Galveston Bay. The much larger peak in deep convective frequency seen in boxes 1 and 2 is likely the result of the UHI effect due to the fact that the sudden increase in deep convective frequency does not occur similarly in box 3, an area equally affected by the sea-breeze but not by the UHI. However, the bay-breeze, which occurs earlier in the day than the sea-breeze, was most likely the cause of the decrease in convection in box 2. More stable air, likely ushered in by the bay-breeze, enters the box 2 domain many hours before entering the box 1 or box 3 domains by the sea-breeze (Pielke 1974).

The total average convergence also supports a role for UHI based on the convergence located over most of Houston and downwind, or north, northeast of Houston (not shown). The total average reflectivity at 2 km does not strongly support the presence of a UHI effect. However, the total average count at 2km does indicate higher frequencies of reflectivities above 30 dBZ over the Houston area than the surrounding areas. At 7 km, the higher reflectivities in the total average reflectivity over the Houston downtown area would indicate the UHI. The count of above 30 dBZ at 7 km strongly indicates the presence of a UHI. This would indicate that the UHI does not affect the convective frequency, but rather the convective intensity, as indicated by the 7 km reflectivity and deep convective count. The increase in the height of convective tops over St. Louis also indicates that UHI affects the intensity of convection (Braham 1981). The downtown and downwind area experienced a far higher frequency of occurrence of deep convection than the surrounding areas.

For comparison, Fig. 12 presents an overlay of deep convective frequency (i.e., counts of occurrence of > 30 dBZ at 7 km from Fig. 8) and a Houston land use map. The high density developed and medium density developed land use are white and light grey, respectively. A large area of deep convective counts greater than 30 encircles the downtown area. Deep convective frequency in this area was greater than 40. Rural and low density areas surrounding Houston averaged 15 to 20 occurrences of > 30 dBZ at 7 km. The influence of the UHI over Houston appears to be sensitive to local changes in land use. Memorial Park is a conservation park in West Houston. The park encompasses 1500 wooded acres , which is double the size of Central Park (New York), and is noted on the map by a large area of dark green just inside the Houston city limits. Despite the park's proximity to Houston, the deep convective frequency over this area only averaged 5 to 10. A park cooling effect was identified in Spronken-Smith and Oke (1998) in which parks in an urban setting averaged 5°C cooler than the surrounding urban setting. The cooler air would cause local divergence over the park setting, inhibiting convection. Higher counts did extend downwind of the city, to the north north-east of the city, and directly north of the east end of the downtown. Steering-level winds for convection most often occur out of the south-southeast and southwest (Shepherd and Burian 2003). Due to this, it would be expected that higher counts would occur downwind of the entire downtown area (i.e., also north of the west end of the downtown). It, therefore, seems possible that the presence of the park is inhibiting the progression of deep convection over and northward of the west side of the city.

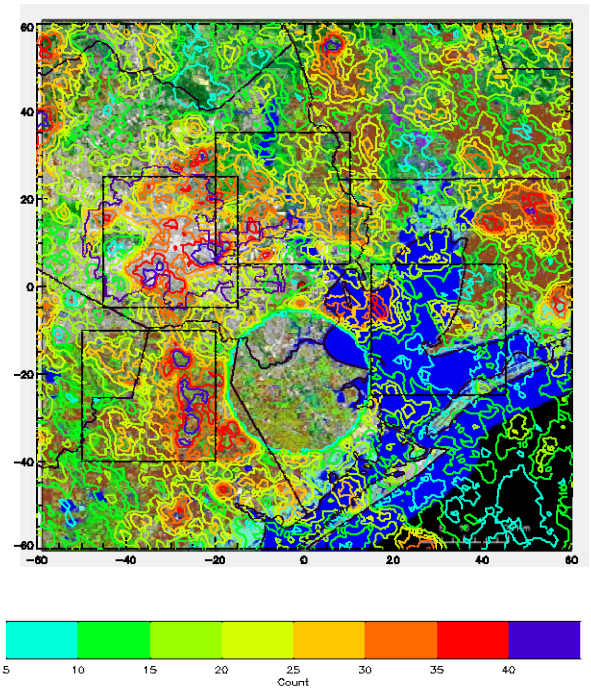


**Fig. 12.** Overlay of Figure 4.31 with a Houston land use map provided by the Texas Commission on Environmental Quality (TCEQ). White is high density developed, light gray is medium density developed, dark grey is low density developed, green is vegetation, brown is crop land, and blue is water.

Fig. 12 also gives insight into convective patterns not associated with Houston. Forested and non-cropland areas shows areas of decreased deep convective frequency, mostly averaging between 5 and 15 counts. Increased counts of > 30 dBZ at 7 km were also present over cultivated herbaceous land (brown). Deep convective frequency here averaged 25 to 40. Increased moisture due to irrigation in these areas is most likely the cause of the increased deep convection,

similar to the findings of Baker et al. (2001). The increased moisture results in a decrease of the height of the LFC which would result in more convection.

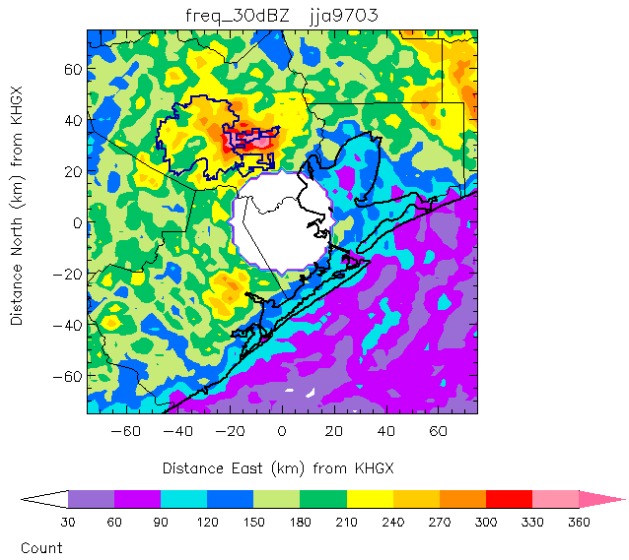


**Fig. 13**. Frequency of >30 dBZ KHGX precipitation echo at 7 km altitude during June-August for the seven year period from 1997-2003.

To investigate the generality of the land use and deep convective frequency result shown in Figs. 8 and 12, we have used the data base of Gauthier et al. (2006) to calculate the frequency of KHGX precipitation echo > 30 dBZ at 7 km altitude for the summer months (June-August) during a seven year period (1997-2003) (Fig. 13). There are distinct similarities and differences between Figs. 8 and 13. Over Houston, the deep convective frequency pattern is shifted somewhat east or east-northeastward in Fig. 13 relative to Fig. 8. In Fig. 13, the deep convective frequency overall maximum is located over the ship channel (i.e., eastern edge of central Houston) and surrounding urban areas while in Fig. 8 it is located more over central to southeastern Houston. Similarly, the interesting minimum in deep convective frequency over Houston is located over Memorial Park in Fig. 8 but is shifted eastward to east-northeastward by 5-10 km in Fig. 13. As a result, it is unclear if the minimum is really associated with Memorial Park or some other mesoscale flow feature that may fluctuate in the mean from year to year (e.g., typical location of Gulf and Bay breezes). Furthermore, the deep convective frequency maximum found in the 2005 study (Fig. 8) within box 3 is largely absent from the 1997-2003 period (Fig. 13). In Fig. 13, there is a noticeable maximum in deep convective frequency that is southeast of box 3. In both periods, the deep convective frequency over the Galveston Bay and Gulf of Mexico is very low compared to Houston and the surrounding rural areas. This simple comparison between the more detailed 2005 results and the longer analysis domain of Gauthier et al. (2006) highlights the need for caution when interpreting small scale convective features from one summer season as being representative of climatological behavior for the Houston area. Nonetheless, the value of the 2005 study is in its ability to more deeply test hypotheses responsible for the overall Houston lightning and rainfall anomalies, which appear to be persistent features from one summer season to the next.

### *4.2 Convergence and Sea-Breeze*

The increased convergence over Galveston Bay during the nighttime hours is produced by a land breeze over the Bay (Aksoy et al. 2005). Convergence was the highest for box 4 between 22 and 5 LST. At 6 LST, with the sunrise, it would be expected that convergence would weaken due to the weakening land-breeze. Shortly after sunrise, a halt of the land breeze and a transition to bay-breeze should occur (Banta et al. 1993). Convection did not begin over this area until just before sunrise at 5 LST and was much weaker than the surrounding domain after 10 LST. Convergence began falling after 5 LST in box 4, while convergence in box 1 began rising after this time.

The box 3 domain is not affected by UHI. Unfortunately, convergence for box 3 is greatly affected by the presence of radar artifacts (not shown). However, the convective pattern in box 3 shows a gradual increase in convection after 10 LST, reaching a peak at 15 to 17 LST. This time frame agrees with the findings of Aksoy et al. (2005). By modeling the sea-breeze, it was found that by 3 pm local time, the most intense convergence moves inland, and by 6 pm a distinct frontal boundary is present. Box 3 is also located adjacent to both the Galveston Bay and the coast. This is an area of cultivated land, though it is more sporadically mixed with forested land than the areas north and east of Galveston Bay. Therefore, it is unlikely that the high levels of convection here are entirely due to irrigation. The interactions of the bay-breeze and the sea-breeze could be providing additional forcing for convection. A similar effect was found by Pielke (1974) involving an enhancement of convection where the lake-breeze from Lake Okeechobee and the Atlantic sea-breeze interact.

A weaker enhancement was located along the northern coast of the Galveston Bay similar to the results of McPherson (1970) and Gibson and Vonder Haar (1990). The maximum occurred along a convex coastline, which has been shown to be an area of increased convergence (Pielke 1974; Baker at al. 2001). The majority of convection at this location occurred between the hours of 5 and 11 LST, with the exception of an isolated event that occurred at 22 and 23 LST. During the early morning time frame, the bay-breeze would have been weak or non-existent (Pielke 1974). Convection would then form along the coast, rather than inland, because the moist air would not be advected away from the coastline by the bay-breeze.

The average winds (e.g., Fig. 14) also revealed the Galveston Bay land-breeze, bay-breeze, and the sea-breeze. The presence of northerly winds over Galveston Bay beginning just after sunset and lasting until 2 LST were due to offshore flow to the Galveston

Bay (Fig. 14). Also, shortly after sunset, nightly bird migration occurs. This migration could result in erroneous northerly winds over the entire domain. The hour of sunrise, and the hour following, was marked by less uniform winds over most of the domain. This corresponds with a time of weakening of the land-breeze. At noon winds began to shift from out of the south near the Bay, likely marking the beginning of the bay-breeze. The lack of an eastward bay-breeze is most likely due to the shallowness of the bay-breeze and the height of the radar beam. A bay-breeze can be limited to less than 500 meters (Abbs 1986). The lowest radar beam would have been near 600 meters above the surface at a distance of 40 kilometers from the radar and, therefore, unable to sample low-level winds and the bay-breeze would be missed.

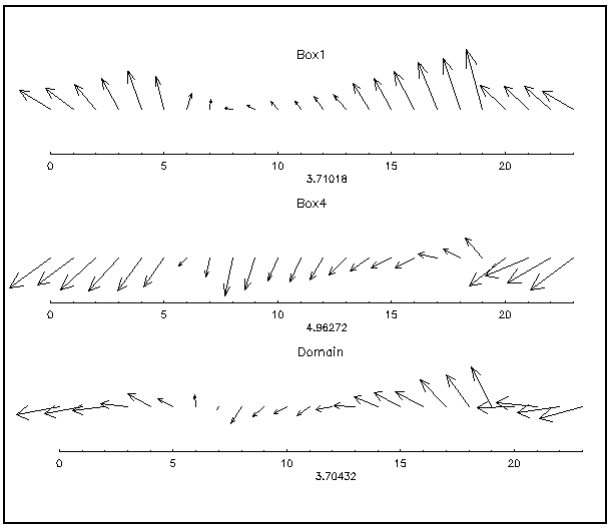


**Fig. 14.** Time series of average boundary layer wind vectors at 0.4 km AGL altitude for box 1, box 4, and the domain. Values under each time series is the maximum average vector for the time series in meters per second. Time on the x-axis is local.

A sea-breeze feature of weak winds out of the southeast began appearing as early as one hour after sunrise in the southern portion of the west dual-Doppler lobe (not shown). A pattern of increasing sea-breeze strength is evident on the time-series image (Fig. 14) and the hourly maps (not shown), steadily increasing after 10 LST. By 15 LST the sea-breeze feature began to appear over Galveston Bay, indicated by more easterly winds. By 17 LST box 4 was characterized by southeasterly wind on average (Fig. 14), indicating the advancement of a deep sea-breeze over Galveston Bay. The difference in the advancement of the sea-breeze between the land and Galveston Bay is due to the weaker temperature gradient over Galveston Bay. This resulted in the slower advancement of the sea-breeze over the bay, which was also identified in Abbs (1986). Based on the time-series (Fig. 14), the sea-breeze reached a peak in strength at 19 LST in box 1. Aksoy et al. (2005) found the peak sea-breeze to occur 9 hours after maximum heating (noon). The wind speed average in box 1 at 20 LST was nearly half the strength of 19 LST. It is important to note that bird migration also begins shortly after sunrise, which can skew the winds to more northerly. However, bird migration does not typically appear in the radar signal until 30 to 45 minutes after sunset, more closely correlating to 21 LST (Shultz 2003, M.S). Therefore, the timing of the weakening of the winds at 20 LST is almost certainly a weakening sea-breeze rather than the appearance of birds. The time of 19 LST correlates more closely with the convection in box 3, which peaked at 18 LST. Boxes 1 and 2 peaked much earlier in the day, at 14 LST. There was a small enhancement at 18 LST, most likely due to the sea-breeze. This would also indicate that the strongest enhancements over boxes 1 and 2 were due mainly to UHI due to the timing of the strong convection in boxes 1 and 2. Had sea-breeze been the main forcing in boxes 1 and 2, the timing of the convection would more closely correspond to the timing of maximum sea-breeze.

### *4.3 Lightning and Convective Strength*

The relationship between lightning and convective strength is examined by the correlation between the amount of convective events with strengths of 30 dBZ or greater at 7 km and the presence of lightning (Larsen and Stansbury 1974, Marshall and Radhakant 1978). With very few exceptions, lightning events correlated with convective strengths greater than 30 dBZ. However, many deep convective events occurred with the presence of little or no lightning. The presence of deep convection appears to be necessary for lightning to occur, but other causative mechanisms must be present. The box 1 and box 2 time-series pattern for the deep convective count closely matches the lightning time-series for the same boxes. The box 3 lightning time-series peak at 18 LST is not matched by a similar peak in the deep convection time-series. By analyzing the frequency maps, it appears that this peak in lightning was caused by a single, large convective event. A correlation between lightning and the total 7 km convective count is also seen on the total images. All significant areas of lightning correlated with high frequencies of deep convection.

### *4.4 The Houston Lightning and Rainfall Anomaly*

The findings of this study support the previous findings of an enhancement in rainfall and lightning over the Houston area. The box 1 and box 2 domains were significantly higher for 2 km average reflectivity, 7 km average reflectivity, 7 km convective frequency, lightning, and average cumulative rainfall than the domain mean. Box 2 was not significantly different than the domain for 2 km frequency while box 1 was significantly higher. The enhanced lightning observed over and downwind of the Houston downtown area in this study was similar in magnitude and location to the results of Orville et al. (2001), Steiger et al. (2002), and Gauthier et al. (2005). However, the magnitude south of Houston (box 3) was found to be more pronounced than the previous studies. However, the length of this study

compared to the previous studies could potentially explain the difference in convection south of Houston.

The enhancement in radar derived rainfall correlates with the location of the enhanced lightning. The rainfall findings also correlate well with the rain-gauge results found by Shepherd and Burian (2003). The maxima in rainfall in the northern portion of the domain do not correlate well with other deep convective features. These maxima may have been produced by a high mean rain rate or a long period of rainfall or both. The enhancement of rainfall, which correlated with an enhancement in lightning, south of the Houston area was also identified by Shepherd and Burian.

Diurnally, box 1 and box 2 were most often significantly higher than the domain mean for the same parameters during the afternoon hours. Most rainfall occurred between the hours of 10 and 19 LST for boxes 1, 2, and 3. Burian and Shepherd (2005) found an increase in rainfall in the Houston urban area and downwind of Houston for the warm season months (June, July, and August) between the hours of 12 and 20 LST.

## 5. CONCLUSIONS

This study further examined the Houston lightning and rainfall anomaly with the use of derived boundary-layer radar parameters along with volumetric radar reflectivity. Mass processing of large amounts of radar data were completed for the months of July, August, and September of 2005 for Houston and Dallas. It was found that the boundary layer winds were not significantly different than other wind observations and were generally useful for scientific analysis (not shown). However, some artifacts, such as bird migration, remained in the radar inferred horizontal winds even after processing and filtering of the data. Hence, care was taken not to interpret these artifacts as meteorological signals.

The results of this study, conducted during one summer season, supported the results of previous findings involving the enhancement of convection over the Houston area. The downtown Houston area, as well as downwind of downtown, had an increase of deep convection, and its associated by-products, namely rainfall and lightning, when compared to the domain mean. More unique to this study was the increase in deep convection, rainfall, and lightning south of the Houston area during the analysis period. This feature was only also identified in the study by Shepherd and Burian (2003). The timing and location of rainfall was also similar to those found in Burian and Shepherd (2005) and Shepherd and Burian (2003).

Based on the findings from this study, it was concluded that the increase in convection over Houston was mostly consistent with the UHI effect. The downtown and downwind area experienced a sudden increase in convection after noon. The downtown area remained higher in frequency until sunset, while the downwind area decreased in frequency shortly after 14 LST. The area to the south of Houston, not affected by UHI effect, exhibited no such sudden increase in convection, but rather a gradual increase in convection up to the time of the strongest sea-breeze signal. Box 1 and box 2 experienced only a small enhancement of convection at that time, indicating a much smaller role for sea-breeze in convection over Houston. Also, the lack of deep convection over Memorial park, an area that would be as equally affected by the sea-breeze as the surrounding Houston area, likely indicates the importance of the UHI in the presence of deep convection. Before we can generalize this latter conclusion, more research is required to fully understand the thermodynamic and dynamic impact of the forested Memorial park area embedded within the larger Houston urban zone on UHI, convective frequency and intensity, lightning, and rainfall.

The relative increase in convection south of Houston during the period of this study appears to be greatly influenced by the sea-breeze. This location may be affected by a convergence zone caused by the collision of the bay-breeze and the sea-breeze. Other areas of increased convection exist over land identified as cultivated herbaceous. The increase in these areas is most likely due to the increase in moisture due to the irrigation present on this land. However, more research and a larger data sample are required to confirm this speculation. As is expected, areas that are labeled as water or forest experienced the least amount of convection (Negri et al. 2004), deep convection, rainfall, and lightning.

This study also found a correlation between high reflectivities at heights above the freezing level (e.g., -10° to -20°C) and the presence of lightning, as suggested by many past studies that are summarized in Vincent et al. (2004). The presence of lightning was co-located with an area of high (> 30 dBZ) reflectivity at temperatures near -10°C (7 km). However, not every area of high reflectivity also had lightning present indicating the importance of microphysics and/or updraft intensity inside the thunderstorms or perhaps that a higher radar reflectivity threshold should have been used (e.g., Vincent et al. 2004).

## 6. REFERENCES


Abbs, D. J., 1986: Sea-breeze interactions along a concave coastline in Southern Australia: Observations and numerical modeling study. *Mon. Wea. Rev.,* **114**, 831-848.

Aksoy, A., F. Zhang, J. W. Nielsen-Gammon, and C. Epifanio, 2005: Ensemble-based data assimilation for thermally forced circulations. *J. Geo. Res.* **110**: doi:10.1029/2004JD005718.

Armijo, L., 1969: A theory for the determination of wind and precipitation velocities with Doppler radars. *J. Atmos. Sci.,* **26**, 570-573.

Banta, R. M., L. D. Olivier, and D. H. Levinson, 1993: Evolution of the Monterey Bay sea-breeze layer as observed by pulsed Doppler lidar. *J. Atmos. Sci.,* **50**, 3959-3982.

Biggerstaff, M. I., L. J. Wicker, J. Guynes, C. Ziegler, J. M. Straka, E. N. Rasmussen, A. Doggett IV, L. D. Carey, J. L. Schroeder, and C. Weiss, 2005: The

shared mobile atmospheric research and teaching radar. *Bull. Amer. Meteor. Soc.,* **86**, 1263-1274.

Braham Jr., R. R., 1981: Urban precipitation processes. *METROMEX: A Review and Summary. Meteor. Monog.*, Amer. Meteor. Soc. **40,** 75-115.

Burian, S. J. and J. M. Shepherd, 2005: Effect of urbanization on the diurnal rainfall pattern in Houston. *Hydrol. Process.,* **19**, 1089-1103.

Cummins, K. L., M. J. Murphy, E. A. Bardo, W. L. Hiscox, R. B. Pyle, and A. E. Pifer, 1998: A combined TOA/MDF technology upgrade of the U.S. National Lightning Detection Network. *J. Geo. Res.,* **103**, 9035-9044.

Cummins, K. L., J. A. Cramer, C. J. Biagi, P. E. Krinder, J. Jerauld, M. A. Uman, and V. A. Rakov, 2006: The U.S. National Lightning Detection Network: Post-upgrade status. *Conf. on Meteor. Appl. of Lightning Data*. Atlanta, GA, *Amer. Meteor. Soc.*

Davies-Jones, R. P., 1979: Dual-Doppler Radar Coverage Area as a Function of Measurements Accuracy and Spatial Resolution. *J. Appl. Meteor.,* **18**, 1229-1233.

Dolan, B. A., and S. A. Rutledge, 2007: An integrated display and analysis methodology for multivariable radar data. *J. Atmos. Oceanic Technol.*, in press.

Gauthier, M. L., W. A. Petersen, L. D. Carey and R. E. Orville, 2005: Dissecting the anomaly: A closer look at the documented urban enhancement in summer season ground flash densities in and around the Houston area. *Geo. Res. Lett*., **32,** doi:10.1029/2005GL022725.

Gauthier, M. L, W. A. Petersen, L. D. Carey, and H. J. Christian, Jr., 2006: The relationship between cloud-to-ground lightning and precipitation ice mass: A radar study over Houston. *Geo. Res. Lett.*, **33**, L20803, doi:10.1029/2006GL027244.

Gibson, H. M. and T. H. Vonder Haar, 1990: Cloud and convection frequencies over the Southeast United States as related to small-scale geographic features. *Mon. Wea. Rev.,* **118**, 2215-2227.

Larsen, H. R. and E. J. Stansbury, 1974: Association of lightning flashes with precipitation cores extending to height 7 km. *J. Atmos. Terr. Phys.,* **36**, 1547-1553.

Marshall, J. S. and S. Radhakant, 1978: Radar precipitation maps as lightning indicators. *J. Appl. Meteor.,* **17**, 206-212.

McPherson, R. D., 1970: A numerical study of the effect of a coastal irregularity on the sea breeze. *J. Appl. Meteor.,* **9**, 767-777.

Miller, J. L., C. G. Mohr, A. J. Weinheimer, 1986: Simple rectification to Cartesian space of folded radial velocities from Doppler radar sampling. *J. Atmos. Oceanic Technol.,* **3**, 162-174.

Miller, J. L., and S. M. Fredrick, 1998: CEDRIC-Custom Editing and Display of Reduced Information in Cartesian Space. Boulder, CO, NCAR Tech. Memo, MMM Division**,** 130.

Oke, T. R., 1987: *Boundary Layer Climates, 2nd. Ed.*, Methuen, 435 pp.

Orville, R. E., G. Huffines, J. Nielsen-Gammon, R. Zhang, B. Ely, S. M. Steiger, S. Phillips, S. Allen, and W. Read, 2001: Enhancement of cloud-to-ground lightning over Houston, Texas. *Geo. Res. Lett.,* **28**, 2597-2600.

Oye, D. and M. Case, 1995: REORDER: a program for gridding radar data. Installation and use manual for the Unix version. Boulder, CO, NCAR Atmospheric Technology Division.

Pielke, R. A., 1974: A three-dimensional numerical model of the sea breezes over South Florida. *Mon. Wea. Rev.,* **102**, 115-139.

Rosenfeld, D., D. B. Wolff, and D. Atlas, 1993: General probability-matched relations between radar reflectivity and rain rate. *J. Appl. Meteor.,* **32**, 50-72.

Schultz, K. W., 2003: An investigation into the contamination of WSR-88D VAD wind profile output by migrating birds. M.S. Thesis. Dept. of Atmospheric Science, College Station, TX, Texas A&M University. 177pp.

Shepherd, J. M., and S. J. Burian, 2003: Detection of urban-induced rainfall anomalies in a major coastal city. *Earth Interaction*, **7**, 1-17.

Spronken-Smith, R. A. and T. R. Oke, 1998: The thermal regime of urban parks in two cities with different summer climates. *Inter. J. Remote Sensing,* **19**, 2085-2104

Steiger, S. M., R. E. Orville, and G. Huffines, 2002: Cloud-to-ground lightning characteristics over Houston, Texas: 1989 - 2000. *J. Geo. Res.,* **107**, 4117-4128.

Vincent, B. R., L. D. Carey, D. Schneider, K. Ketter, and R. Gonski, 2004: Using WSR-88D reflectivity data for the prediction of cloud-to-ground lightning: A central North Carolina study. *Natl. Weather. Dig.* **27**, 35-44.

## 7. ACKNOWLEDGEMENTS

This research was funded in part by grants from TCEQ (582-5-64593-FY05-01 and 582-5-64953-FY06-11, HARC (H-56-2005-T2-TAMU)), and NSF (ATM-0442011). We acknowledge the outstanding engineering, logistical, moral support, and tireless efforts of Mr. Jerry Guynes. We acknowledge the hard work by all of the radar operators (too numerous to list here) during round the clock shifts on the SMART radars during TexAQS II 2005. We thank the administrative staff in the Department of Atmospheric Sciences at Texas A&M University for their outstanding logistical and travel support during a challenging field deployment. Finally, we thank Dr. John Nielsen-Gammon and Dr. Fuqing Zhang for their helpful feedback on this research.